

**Supplementary Information for
Kurarinone alleviated Parkinson's disease *via* stabilization of
epoxyeicosatrienoic acids in animal model**

Cheng-Peng Sun^{a,+}, Jun-Jun Zhou^{a,+}, Zhen-Long Yu^a, Xiao-Kui Huo^a, Juan Zhang^a, Christophe Morisseau^b, Bruce D. Hammock^{b,*}, Xiao-Chi Ma^{a,*}

Bruce D. Hammock and Xiao-Chi Ma
Email: bdhammock@ucdavis.edu (B.D. Hammock); maxc1978@163.com

This PDF file includes:

Supplementary text
Figures S1 to S14
Tables S1 and S6
SI References

Supplementary Information

Materials and Methods.

Materials. The primary antibodies COX-2, p65, p-p65, and p-GSK3 β were purchased from Cell Signaling Technology (CST, Danvers, MA, USA). The primary antibodies TH, GSK3 β , and sEH were purchased from ABclonal (Wuhan, China). The primary antibodies β -actin, IL-6, and TNF- α were purchased from Proteintech (Wuhan, China). DA, DOPAC, HVA, and MPTP were purchased from Sigma Aldrich (St. Louis, Missouri, USA). 8,9-EET, 11,12-EET, 14,15-EET, 8,9-DHET, 11,12-DHET, and 14,15-DHET were purchased from Cayman Chemical (Ann Arbor, Michigan, USA).

Plant material and extract preparation. The rhizomes of *S. flavescens* were purchased from Beijing Tongrentang (Beijing, China), and identified by Prof. Jing-Ming Jia (Shenyang Pharmaceutical University). A voucher specimen (SF201806) has been deposited in the herbarium of the Department of Medicinal Chemistry, Dalian Medical University.

S. flavescens powder (capable of passing a 4-mm sieve) was extracted with 95% EtOH at 90 °C for 2 h. After removing the solvent, the residue was stored at 4 °C.

The extract of *S. flavescens* were isolated by an ODS column and eluted with MeOH-H₂O (10%-90%) to afford five fractions (Fr. 1-Fr. 5). Fr. 5 was separated by preparative HPLC (75% MeOH-H₂O) to afford kurarinone (562 mg). Its structure was identified by ¹H and ¹³C NMR spectra.

Animals. Male C57BL/6 mice (23-25 g, 8 weeks) were afforded from the Experimental Animal Center of Dalian Medical University (Dalian, China). sEH KO mice (21-24 g) with targeted deletion of sEH gene (*Ephx2*) which is backcrossed to C57BL/6 background were used. All animal experiments were in accordance with the Institutional Animal Care and Use Committee of Dalian Medical University. All the animals were kept under a light/dark cycle of 12 h per day at a controlled temperature of 22-24 °C and 50-60% humidity with water and food *ad libitum*.

Experimental procedure. The mouse model of MPTP-induced PD was used to investigate the protective effect of the extract of *S. flavescens* (SFE) and kurarinone.

First, mice were randomly divided into four groups (10 mice/group): the control group (only administrated with vehicle), SFE (100 mg/kg) group, MPTP (20 mg/kg) group, and MPTP + SFE (100 mg/kg) group. Mice in SFE group or MPTP + SFE group were administrated with SFE (100 mg/kg, dissolved in 10% hydroxypropyl- β -cyclodextrin, i.g.) for 19 days, and Mice in MPTP group or MPTP + SFE group were administrated with MPTP (20 mg/kg, dissolved in saline, i.p.) from the 8th day to the 12th day. The control group was administrated with saline (i.p.) and 10% hydroxypropyl- β -cyclodextrin (i.g.).

Second, mice were randomly divided into six groups (10 mice/group): the control group (only administrated with vehicle), kurarinone (20 mg/kg) group, MPTP (20 mg/kg) group, MPTP + kurarinone (5 mg/kg) group, MPTP + kurarinone (10 mg/kg) group, and MPTP + kurarinone (20 mg/kg) group. The mice in kurarinone group or MPTP + kurarinone group were administrated with kurarinone (5, 10, or 20 mg/kg, dissolved in 10% hydroxypropyl- β -cyclodextrin, i.g.) for 19 days, and Mice in MPTP group or MPTP + kurarinone group were administrated with MPTP (20 mg/kg, dissolved in saline, i.p.) from the 8th day to the 12th day. The control group was administrated with saline (i.p.) and 10% hydroxypropyl- β -cyclodextrin (i.g.).

Third, wild-type (WT) and sEH knockout (KO) mice were randomly divided into four groups (10-12 mice/group): the MPTP-treated WT group (12 mice/group; MPTP, 20 mg/kg), the MPTP-treated + kurarinone WT group (12 mice/group, MPTP, 20 mg/kg; kurarinone, 20 mg/kg), the MPTP-treated KO group (10 mice/group; MPTP, 20 mg/kg), and the MPTP-treated + kurarinone KO group (11 mice/group, MPTP, 20 mg/kg; kurarinone, 20 mg/kg). Mice in MPTP WT and KO groups or MPTP + kurarinone WT and KO groups were administrated with kurarinone (20 mg/kg, dissolved in 10% hydroxypropyl- β -cyclodextrin, i.g.) for 19 days and MPTP (20 mg/kg, dissolved in saline, i.p.) from the 8th day to the 12th day.

Forth, mice were randomly divided into three groups (10 mice/group): the control group (only administrated with vehicle), MPTP (20 mg/kg) group, and MPTP + kurarinone (20 mg/kg) group. Mice in MPTP group and MPTP + kurarinone group were administrated with MPTP (20 mg/kg,

dissolved in saline, i.p.) for 5 days, after 1 h of MPTP administration, mice in MPTP + kurarinone group were administrated with kurarinone (20 mg/kg, dissolved in 10% hydroxypropyl- β -cyclodextrin, i.g.) for 12 days. The control group was administrated with saline (i.p.) and 10% hydroxypropyl- β -cyclodextrin (i.g.).

Fifth, mice were randomly divided into three groups (10 mice/group): the control group (only administrated with vehicle), ROT (rotenone, 2 mg/kg) group, and ROT + kurarinone (20 mg/kg) group. Mice in ROT group and ROT + kurarinone group were administrated with ROT (2 mg/kg, dissolved in 7.5% PEG400, i.p.) for 15 days, after 1 h of ROT administration, mice in ROT + kurarinone group were administrated with kurarinone (20 mg/kg, dissolved in 10% hydroxypropyl- β -cyclodextrin, i.g.) for 18 days. The control group was administrated with saline (i.p.) and 10% hydroxypropyl- β -cyclodextrin (i.g.).

Behavioral assessment-catwalk gait analysis. The Catwalk automated gait analysis system (Noldus, Wageningen, Netherlands) was used to assess the gait and motor coordination from the 15th day to the 19th day according to our previous method.

LC-MS/MS analysis. The levels of DA, DOPAC, HVA, 8,9-EET, 11,12-EET, 14,15-EET, 8,9-DHET, 11,12-DHET, and 14,15-DHET in STR were determined by LC-MS/MS based on the previous methods (1, 2). STR tissues were weighed, homogenized in the ice-water bath, and then centrifuged at 20000 *g* for 20 min. The supernatant was collected, and then analyzed using a multiple reaction monitoring (MRM) method and an AB Sciex Qtrap® 5500 LC-MS/MS system (Foster City, CA, USA). The levels of DA, DOPAC, HVA, 8,9-EET, 11,12-EET, 14,15-EET, 8,9-DHET, 11,12-DHET, and 14,15-DHET were calculated based on their respective standard curves.

Identification of effective components in mouse plasma and brain. Mice received a single oral dose of *S. flavescens* extract (100 mg/kg, dissolved in 10% hydroxypropyl- β -cyclodextrin). Blood and brain were collected after 30 min. Plasma samples were obtained by centrifugation at 3500 rpm for 10 min under 4°C. Brain specimens were homogenized in water. Then, the plasma and brain homogenate were subjected to liquid-liquid extraction using ethyl acetate. The organic phase was evaporated to dryness by nitrogen at 37°C and redissolved using 100 μ L of acetonitrile: H₂O (35:65, v/v, containing 0.1 % formic acid). The supernatant (10 μ L) of each sample was injected into the UPLC-LC/MS/MS system for analysis.

Absorbed prototype components in mouse plasma and brain were quantitatively analyzed by liquid chromatography tandem mass spectrometry (LC-MS/MS, AB SciexQtrap® 5500 LC-MS/MS system). Chromatographic separation was performed on Xbridge BEH C18 (2.1 \times 150 mm, 2.5 μ m) at 30°C. The mobile phase was composed of A (water containing 0.1% formic acid) and B (acetonitrile) with a gradient elution of 35% B at 0–5 min, 60% B at 10–20 min, 90% B at 25–30 min, 35% B at 31–35 min. The flow rate was 0.25 mL/min. The detection was performed by Q1 full scan in negative ionization mode. The source parameters were set as follows: Ion spray voltage, -4.5 kV; Temperature, 300°C; Gas source 1, 55 psi; Gas source 2, 65 psi. The *m/z* range were set as 200–600 Da. Data acquisition was performed with Analyst® 1.6.2 Software.

Identification of targets of kurarinone by the TPP approach. The SN sections of PD mice were lysed using PBS (pH 7.4) containing 1% EDTA-free cocktail to afford the soluble proteins after centrifuging at 20,000 *g* for 10 min at 4 °C. The supernatant was divided into two aliquots, one aliquot was treated with 200 μ M kurarinone (dissolved in DMSO) and the other aliquot was treated with an equivalent amount DMSO alone as vehicle. After the incubation of the protein extract with kurarinone or DMSO for 30 min at room temperature using rotometer at 10 rpm rotating speed, the above two mixtures were divided into five aliquots of 50 μ L, respectively. The replications in vehicle and kurarinone-treated groups were heated individually at 52°C for 3 min, followed by cooling at room temperature for 3 min. The heated lysates were subjected to centrifugation at 20,000 *g* for 20 min at 4°C to separate soluble proteins from precipitated proteins. Supernatants were collected for quantitative proteomics analysis. The protein concentration was determined by BCA protein assay kit (Thermo Fisher Scientific, San Jose, CA, USA).

For the validation of sEH based on western blotting analysis by TPP, the two portions of SN lysate incubated with DMSO or 200 μ M kurarinone were divided into seven aliquots, respectively.

All the aliquots were heated individually at different temperatures for 3 min. After cooling at room temperature for 3 min, soluble fraction was obtained by centrifugation as described above and used for western blotting.

Targets identification of kurarinone by SIP approach. SN lysates were incubated with DMSO or kurarinone as described in the TPP method. The five replications in vehicle or kurarinone-treated groups were treated with an organic solvent mixture of acetone: ethanol: acetic acid (A.E.A., 50: 50: 0.1) to reach the final percentage of solvent mixture to 12%. Subsequently, the mixtures were equilibrated at 800 rpm for 20 min at 37 °C. Supernatants were collected after the mixtures were centrifuged at 20,000 g for 10 min at 4 °C and used for quantitative proteomics analysis.

For the validation of sEH based on western blotting analysis by SIP, the SN lysates were incubated with DMSO or 200 μ M kurarinone for 30 min. Seven aliquots were prepared for each sample and treated with A.E.A. to reach different final percentages. After equilibration, the soluble fraction was obtained by centrifugation as described above and used for western blotting.

Sample preparation for MS analysis. Equal volume of supernatants incubated with DMSO or kurarinone were denatured with 8 M guanidine in 50 mM HEPES (pH 8.0), followed by addition of 10 mM tris-(2-carboxyethyl) phosphine (TCEP) and 40 mM chloroacetamide (CAA) at 95 °C for 5 min for the reduction of disulfide bonds and alkylation of reduced cysteine. Digestion of proteins were processed with filter-aided sample preparation (FASP) technique. Briefly, above denatured proteins in vehicle and kurarinone-treated groups were concentrated and washed two times with 20 mM Ammonium Bicarbonate (pH 8.0) using 10k ultrafiltration tube (Sartorius AG, Germany) under the condition of 14,000 g at 4°C. Subsequently, the trypsin was added to the samples at a ratio of 1: 20 (enzyme/protein, w/w) for digestion at 37 °C for 16 h. Finally, the resulted peptides were lyophilized in a SpeedVac (Thermo Fisher Scientific, San Jose, CA, USA) and stored at -80 °C before use.

LC-MS/MS analysis. The analysis of tryptic peptides was performed on a Ultimate 3000 RSLCnano system coupled with a Q-Exactive-HF mass spectrometer, controlled by Xcalibur software v2.1.0 (Thermo Fisher Scientific, Waltham, MA, USA). The peptides were resolved in 0.1% formic acid/water, and were quantified by using NanoDrop 2000 (Thermo Fisher Scientific, USA). And then iRT standard peptide mix (Biognosys, Switzerland) was added to injection-ready peptide samples at a ratio of 1:10 (v/w). Briefly, 1 μ g of the re-suspended peptides were automatically loaded onto a C18 trap column at a flow rate of 5 μ L/min. The capillary analytical column (150 μ m i.d.) was packed in-house with 1.9 μ m C18 ReproSil particles (Dr. Maisch GmbH). The mobile phase A and B were 0.1% FA and 80% ACN/0.1% FA, respectively. The flow rate was set as 600 nL/min. The gradient of the mobile phase was developed as follows: 12-30% mobile phase B for 58 min; 30-45% B for 12 min; 45-90% B for 3 min; 90% B was maintained for 7.5 min; 90-2% B for 0.5 min; and finally equilibration with 98% mobile phase A for 8 min.

The LC-MS/MS system was operated in data-independent MS/MS acquisition mode. The full mass scan acquired in the Orbitrap mass analyzer was from m/z 350 to 1050 with a resolution of 60,000 (m/z 200), MS/MS spectra of DIA data were acquired in the Orbitrap as well with a 30,000 resolution (m/z 200). The automatic gain control (AGC) target and the maximum inject time were set to 3e6 and 20 ms. DIA experiments were performed using different isolation window settings (see sheet 1) to acquire the data. The target value for fragment scans was set at 1e6 with a maximum fill time of 50 ms for each DIA experiment.

Protein identification and quantification. DIA files were processed with Spectronaut with default settings in library-free mode, except that trypsin was set as the proteolytic enzyme.

Data processing. The data exported from Spectronaut was analyzed using excel software. T-student test was performed to determine statistical significance of proteins. The proteins that were identified both in TPP and SIP methods were used for the comparison of P values. The proteins with -log₁₀ P value > 3.5 were considered as the finally potential protein targets of Shk. The scatter plots were carried out by Graphpad Prism 7 software (Graphpad Software, Inc, La Jolla, CA).

Western blot analysis. SN were lysed with western IP cell/tissue lysis buffer (Beyotime Institute of Biotechnology, Shanghai, China) containing PMSF (Sigma) on ice for 30 min. Equal amounts of protein (30 µg/ sample) were separated by SDS-PAGE on 10% gel electrophoresis and transferred onto 0.45 µm PVDF membranes (GE Healthcare Life Sciences, Pittsburgh, PA, USA). 0.5% BSA (Sigma) was used at room temperature for 2 h to block the membranes. The following monoclonal primary antibodies were used for western blot analysis overnight at 4 °C: anti-COX-2 (1:1000), anti-p65 (1:1000), anti-p-p65 (1:1000), anti-p-GSK3β (1:1000), anti-TH (1:1000), anti-GSK3β (1:1000), anti-sEH (1:1000), anti-IL-6 (1:1000), anti-TNF-α (1:1000), and anti-β-actin (1:1000). The membranes were washed three times with Tris-buffered saline with 0.1% Tween 20 for 10 min each at room temperature. The membranes were incubated with anti-rabbit immunoglobulin IgG and anti-mouse IgG (both 1:5000; both from Proteintech Group) horseradish peroxidase-conjugated secondary antibodies at room temperature for 1 h. The signal was visualized with chemiluminescence kit (BeyoECL Plus; Beyotime Institute of Biotechnology). The intensities of band signals were quantified using Quantified One densitometric software (Bio-Rad Laboratories, Inc.). The relative intensity of the target bands was normalized to that of β-actin. Experiments were repeated at least three times.

Immunohistochemistry staining. Mouse brains were fixed with 4% paraformaldehyde, and 20% and 30% sucrose solution for 24 h, successively. SN and STR samples were cut into 20 µm thick sections (Leica, Germany) for the immunohistochemistry or immunofluorescence assay. The STR sections were blocked with 10% goat serum at 37 °C for 1.5 h, and then were conjugated with primary antibodies TH (1:200) at 4 °C overnight. After the sections was washed with PBS for three times, they were incubated with a horseradish peroxidase-conjugated secondary antibody at 37 °C for 30 min, and then stained with DAB kit (Beyotime, Shanghai, China).

Immunofluorescence staining. The SN sections were blocked with 10% goat serum in 0.3% Triton-100/PBS at 37 °C for 1.5 h, and then were incubated with the primary antibodies Iba-1 (1:100) and TH (1:200) at 4 °C overnight. After the sections was washed with PBS for three times, they were conjugated to the secondary antibody CoraLite 594 at 37 °C for 1.5 h.

sEH expression and purification. The sEH gene (from 230 to 555) was inserted into the pET3a expression vector. The protein was overexpressed in the *E. coli* Rossetta (DE3) strain by initially growing cells at 37 °C to an absorbance of 0.8 at A₆₀₀, and inducing by addition of 0.5 mM IPTG and overnight growth at 16 °C. Cells were disrupted by sonication in buffer A (20 mM Tris/HCl (pH 8.0), 350 mM NaCl, and 1 mM PMSF) and the supernatant applied to a nickel column equilibrated with buffer A, washed with buffer A, and the sEH protein eluted with 250 mM imidazole in buffer A. sEH-containing fractions were concentrated by microfiltration and applied to a Superdex-200 gel-filtration column in buffer B (10 mM Tris/HCl (pH 8.0), 100 mM NaCl, 1 mM DTT). Purified sEH was judged to be greater than 99% pure by SDS-PAGE and concentrated by microfiltration to 10 mg/mL.

Inhibition study. The inhibition of sEH by kurarinone was determined as described using either *trans*-diphenyl propene oxide (t-DPPO), (3-Phenyl-oxiranyl)-acetic acid cyano-(6-methoxy-naphthalen-2-yl)-methyl ester (PHOME) or cyano(6-methoxy-naphthalen-2-yl)methyl *trans*-[(3-phenyloxiran-2-yl)methyl] carbonate (MNPC) as substrate (3).

Crystallization and structure determination. Crystals of sEH grown using hanging drop vapor diffusion by mixing equal volumes of protein and a buffer solution containing 1.26 M Sodium phosphate monobasic monohydrate, 0.14 M Potassium phosphate dibasic at temperature 291 K. Crystals were rapidly soaked in the reservoir solution supplemented with 20% glycerol as cryo-protectant, mounted on loops, and flash-cooled at 100 K in a nitrogen gas cryo-stream. Crystals diffraction data was collected from a single crystal at Shanghai Synchrotron Radiation Facility (SSRF) BL18U beamline, China, with a wavelength of 0.9793 Å at 100 K. The diffraction data were processed and scaled with HKL-3000 (4). Relevant statistics were summarized in Table S1. The structure was solved by the molecular replacement method and *Pseudomonas aeruginosa* HDAH (PDB entry 5G12) was used as the starting model (5). Initial model was build using PHENIX.autobuild (6). Manual adjustment of the model was carried out using the program COOT

(7) and the models were refined by PHENIX. refinement (6) and Refmac5 (8). Stereochemical quality of the structures was checked by using PROCHECK (9). All of residues locate in the favored and allowed region and none in the disallowed region. The coordinates of kurarinone and sEH have been deposited with the Rutgers Collaborative Structural Bioinformatics database (Protein Data Bank) under accession number 7EBA.

Statistical analysis. All data were analyzed using GraphPad Prism 8 (GraphPad Software Inc., San Diego, CA, USA). Results were presented as means \pm SEM. The significance of difference was determined by one-way analysis of variance (ANOVA) or two-way ANOVA, followed by Tukey's test. Difference was considered significant at $p < 0.05$.

Identification of kurarinone. Kurarinone was isolated as powders. Its ^1H NMR data (Table S6) displayed four aromatic signals at δ_{H} 7.21 (1H, d, $J = 8.3$ Hz, H-6'), 6.33 (1H, d, $J = 2.2$ Hz, H-3'), 6.25 (1H, dd, $J = 8.3, 2.2$ Hz, H-5'), and 6.12 (1H, s, H-6), three olefinic signals at δ_{H} 4.90 (1H, m, H-4''), 4.56 (1H, m, H-9''a), and 4.48 (1H, d, $J = 2.2$ Hz, H-9''b), one methoxy signal at δ_{H} 3.70 (3H, s, OCH₃-5), and three methyl signals at δ_{H} 1.58 (3H, s, CH₃-10''), 1.53 (3H, s, CH₃-7''), and 1.44 (3H, s, CH₃-6''). The ^{13}C NMR (Table S3) data of kurarinone showed 26 carbon signals, including one carboxyl carbon at δ_{C} 188.9 (C-4), twelve aromatic carbons at δ_{C} 162.4 (C-5), 162.0 (C-7), 159.6 (C-4a), 158.1 (C-4'), 155.2 (C-2'), 127.2 (C-6'), 116.3 (C-1'), 106.9 (C-8), 106.2 (C-5'), 104.3 (C-8a), 102.3 (C-3'), and 92.4 (C-6), four olefinic carbons at δ_{C} 147.9 (C-8''), 130.6 (C-5''), 123.4 (C-4''), and 110.7 (C-9''), and one methoxy carbon at δ_{C} 55.2 (OCH₃-5). These above data were identical with those of authentic kurarinone (10), accordingly, this compound was defined as kurarinone. It also showed one spot on TLC in several solvent systems, one peak on LC MS with UV and with total ion monitoring, and a mass fragmentation pattern consistent with the structure and identical to the standard compound.

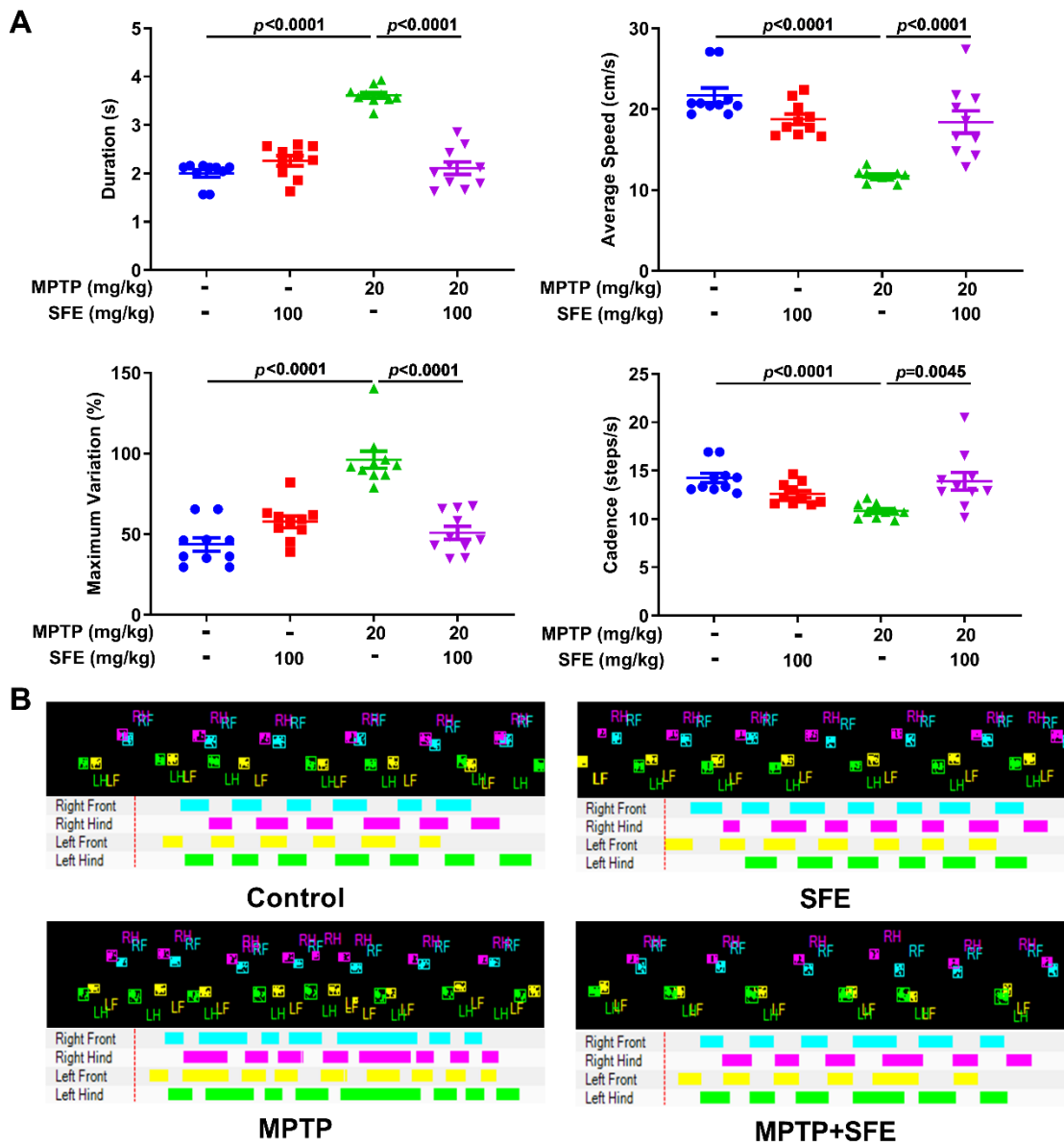


Figure S1 SFE alleviated the behavior of MPTP-induced PD mice. (A) The behavioral parameters. Data represent mean \pm SEM, $n = 10$. The significance was determined by one-way ANOVA followed by Tukey's test. (B) The representative footprints.

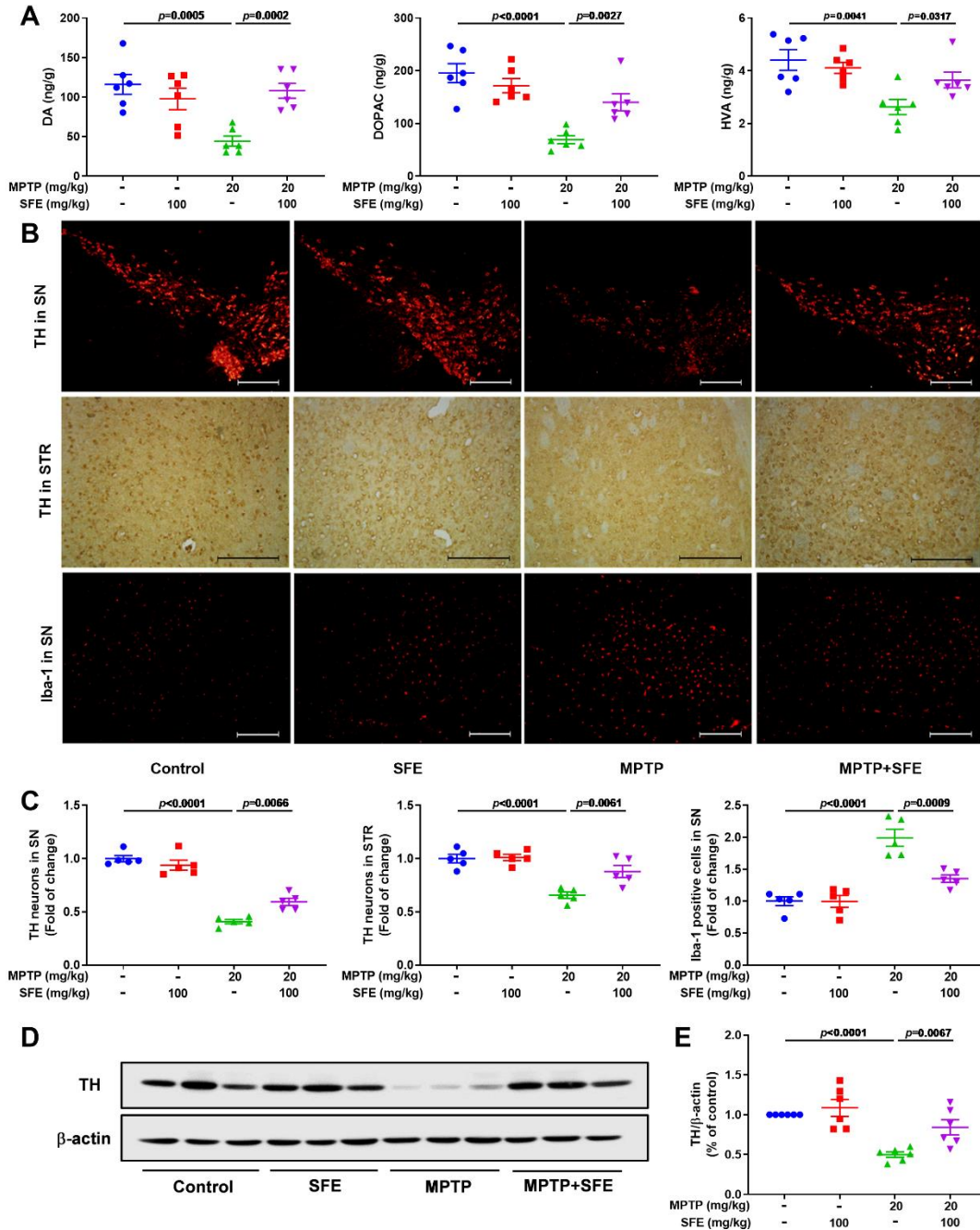


Figure S2 SFE enhanced key neurotransmitter levels, TH expression level, and inhibition of the activation of microglial cells in MPTP-induced PD mice. (A) Effects of SFE on neurotransmitters DA, DOPAC, and HVA. Data represent mean \pm SEM, $n = 6$. The significance of difference was determined by one-way ANOVA followed by Tukey's test. (B) The representative staining of TH in SN and STR and Iba-1 in SN. (C) The data of TH neurons in SN and STR, and Iba-1 positive cells in SN. Data represent mean \pm SEM, $n = 5$. The significance of difference was determined by one-way ANOVA followed by Tukey's test. (D) Effect of SFE on TH expression level in SN. (E) Quantitative data of TH. Data represent mean \pm SEM, $n = 6$. The significance of difference was determined by one-way ANOVA followed by Tukey's test.

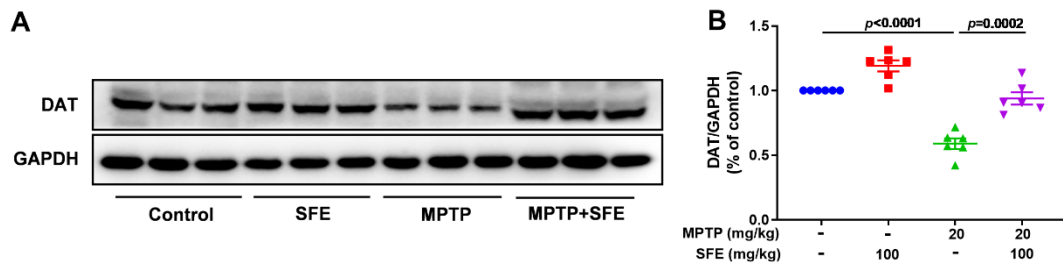


Figure S3 SFE enhanced DAT expression level in MPTP-induced PD mice. (A) Effect of SFE on DAT expression level in STR. (B) Quantitative data of DAT. Data represent mean \pm SEM, $n = 6$. The significance of difference was determined by one-way ANOVA followed by Tukey's test.

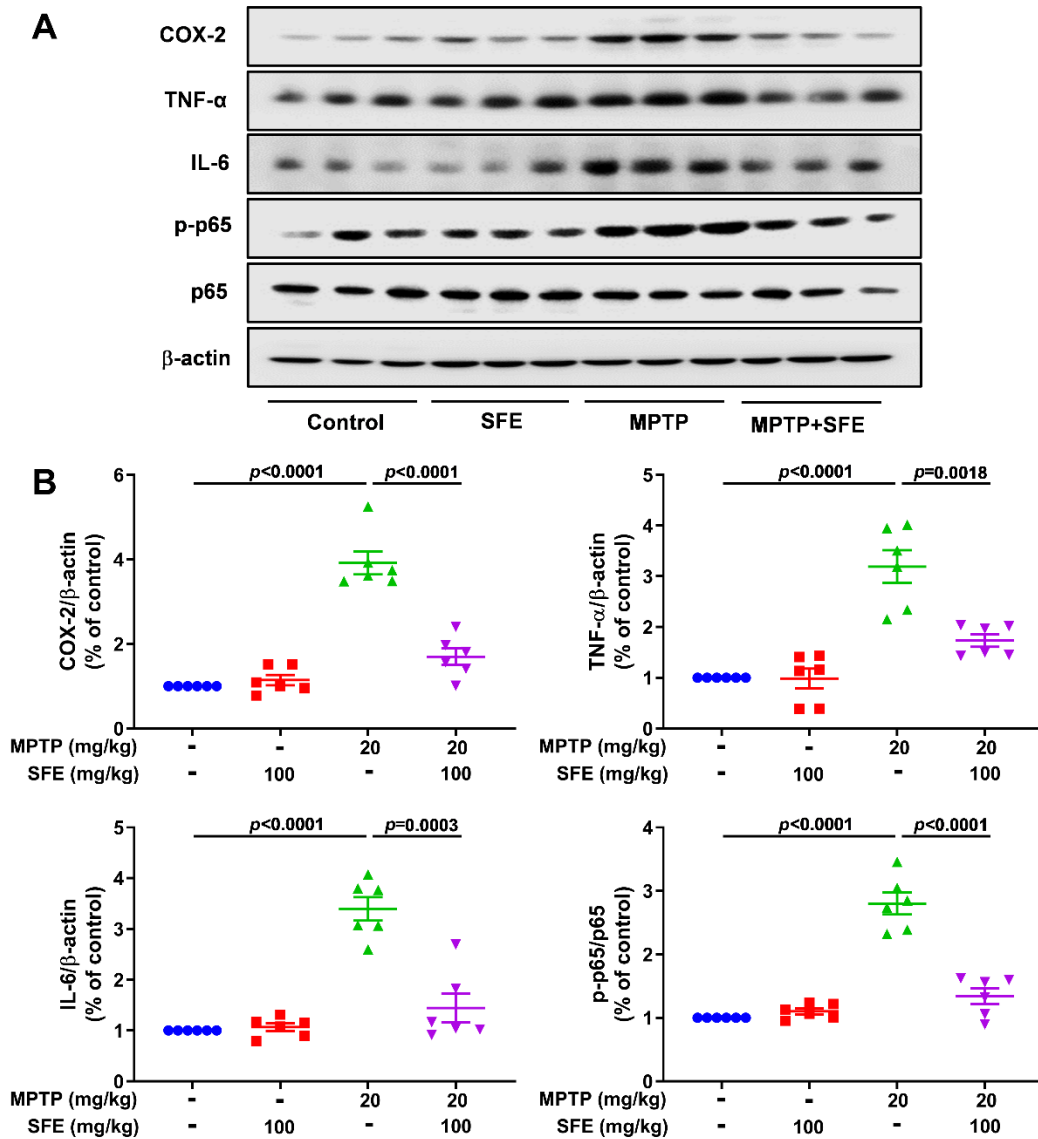


Figure S4 SFE alleviated the neuroinflammation via NF- κ B signaling pathway in MPTP-induced PD mice. (A) Effects of SFE on expression levels of COX-2, TNF- α , IL-6, p-p65, and p65. (B) Quantitative data of COX-2, TNF- α , IL-6, and p-p65/ p65. Data represent mean \pm SEM, n = 6. The significance of difference was determined by one-way ANOVA followed by Tukey's test.

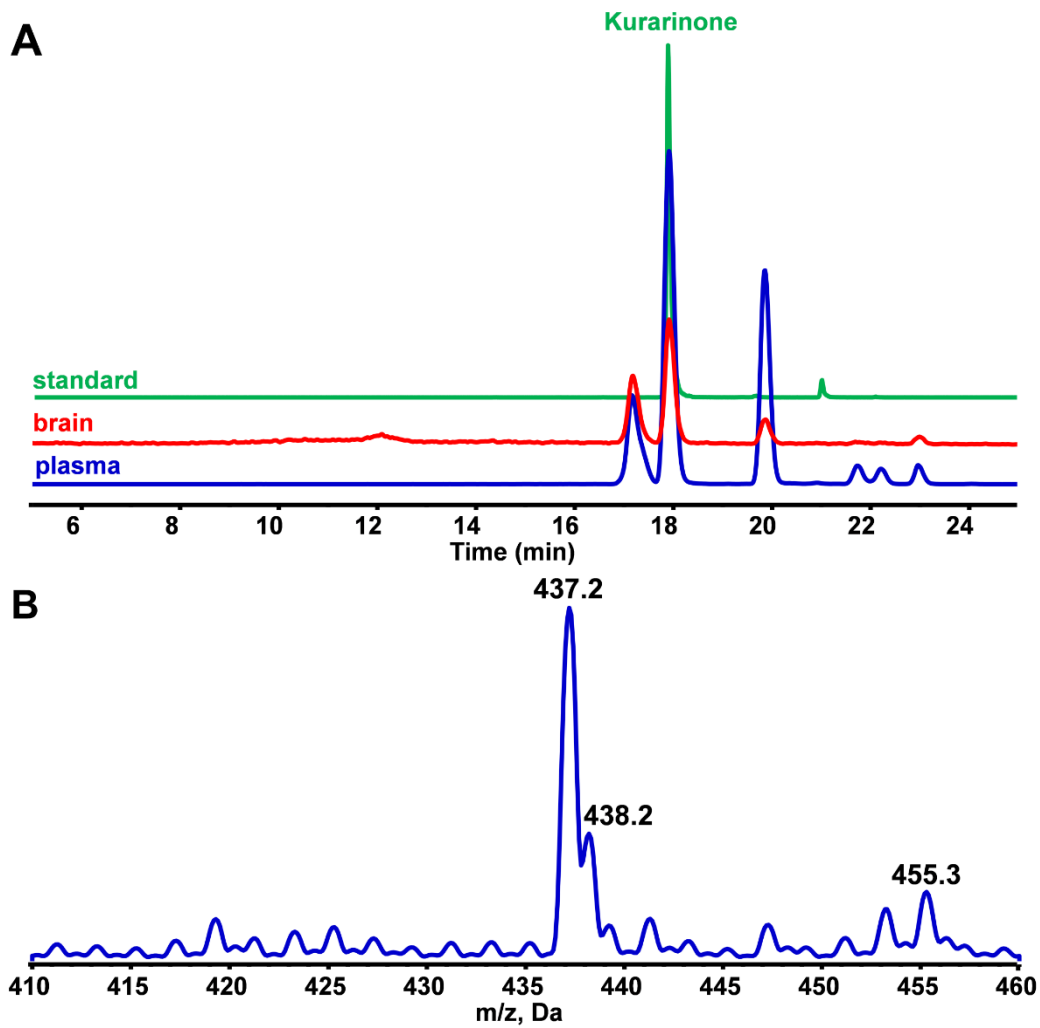


Figure S5. Representative total ion chromatogram of plasma and brain in negative ion mode after administration of SFE for 20 min. Mice were orally administered SFE (100 mg/kg) and sacrificed after 20 min. Plasma and brain were collected for LC-MS analysis. (A) The total ion chromatogram (m/z 200-600 Da) in negative ion mode was obtained by deduction of the signal of the blank samples. (B) The MS plot of standard kurarinone in negative ion mode.

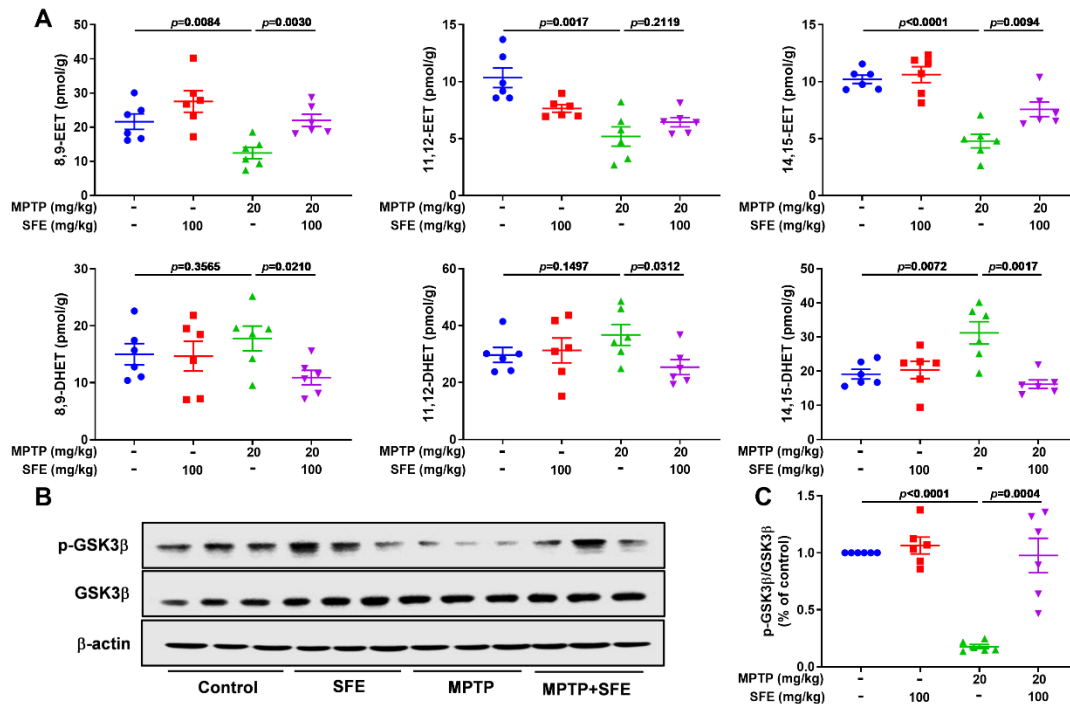


Figure S6 SFE alleviated the increase of sEH activity and suppressed the GSK3β signaling pathway *via* stabilizing the level of EETs in MPTP-induced PD mice. (A) Effect of SFE on 8,9-EET, 11,12-EET, 14,15-EET, and their corresponding diols 8,9-DHET, 11,12-DHET, and 14,15-DHET in MPTP-induced PD mice. Data represent mean ± SEM, n = 6. The significance was determined by one-way ANOVA followed by Tukey's test. (B) Effects of SFE on p-GSK3β and GSK3β expression levels in MPTP-induced PD mice. (C) Quantitative data of p-GSK3β/GSK3β. Data represent mean ± SEM, n = 6. The significance was determined by one-way ANOVA followed by Tukey's test.

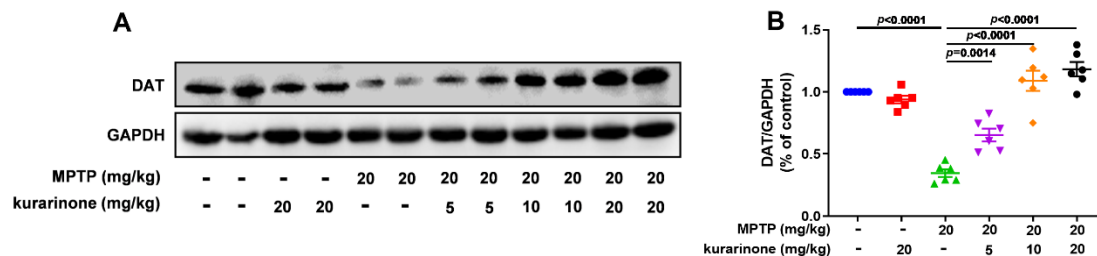


Figure S7 Kurarinone enhanced DAT expression level in MPTP-induced PD mice. (A) Effect of kurarinone on DAT expression level in STR. (B) Quantitative data of DAT. Data represent mean ± SEM, n = 6. The significance of difference was determined by one-way ANOVA followed by Tukey's test.

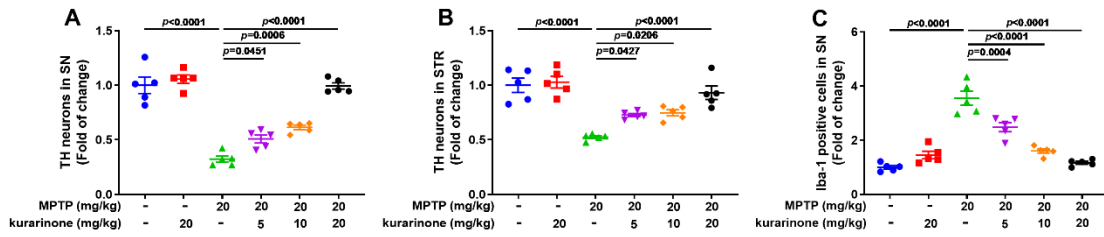


Figure S8 Kurarinone enhanced TH neurons in SN and STR, and reduced microglial activation in SN of MPTP-induced PD mice. (A) The data of TH neurons in SN. Data represent mean \pm SEM, n = 5. The significance was determined by one-way ANOVA followed by Tukey's test. (B) The data of TH fibers in STR. Data represent mean \pm SEM, n = 5. The significance was determined by one-way ANOVA followed by Tukey's test. (C) The data of Iba-1 positive cells in SN. Data represent mean \pm SEM, n = 5. The significance was determined by one-way ANOVA followed by Tukey's test.

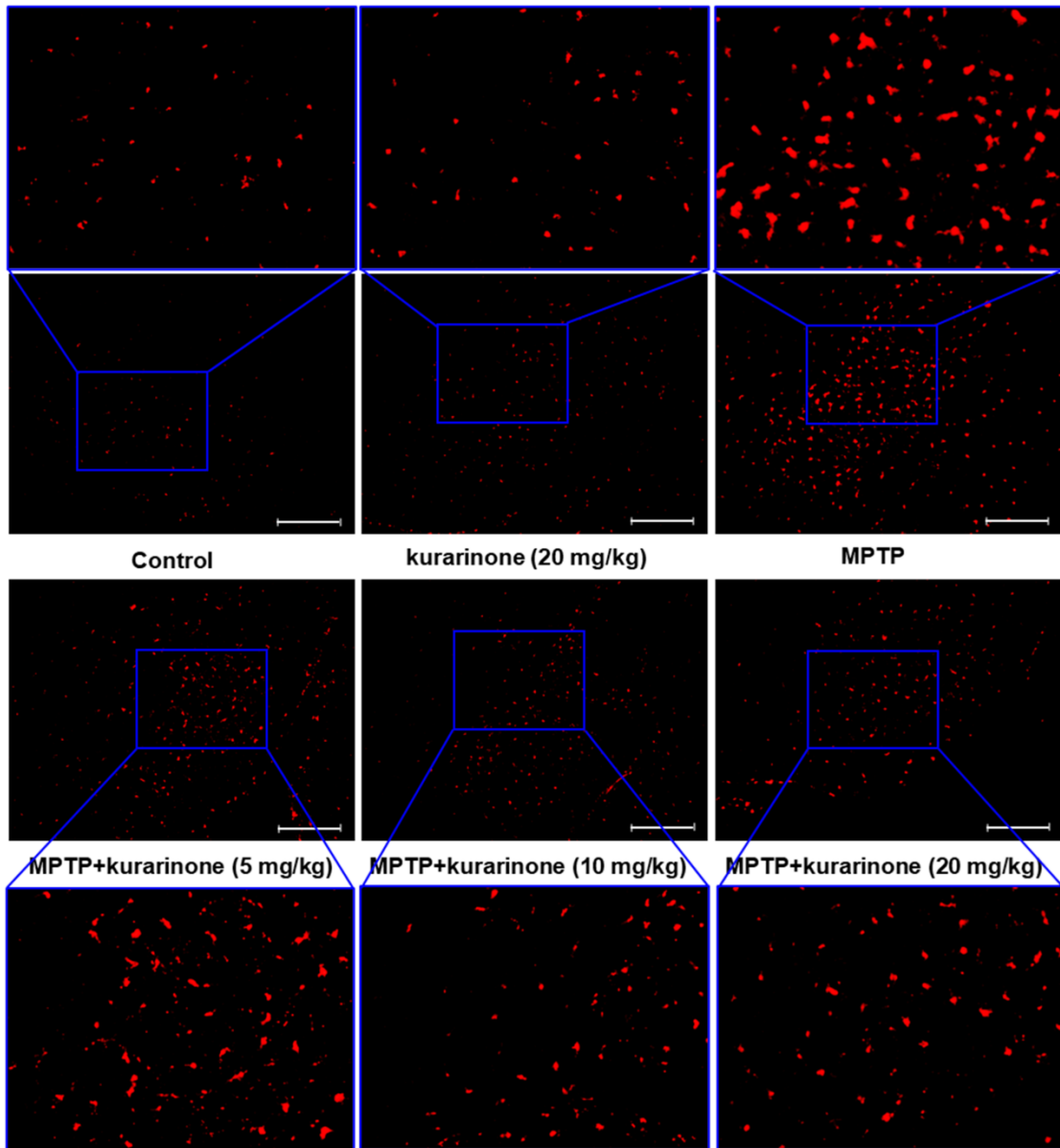


Figure S9 Kurarinone from *S. flavescens* inhibited the activation of microglial in MPTP-induced PD mice. The representative staining of Iba-1 in SN.

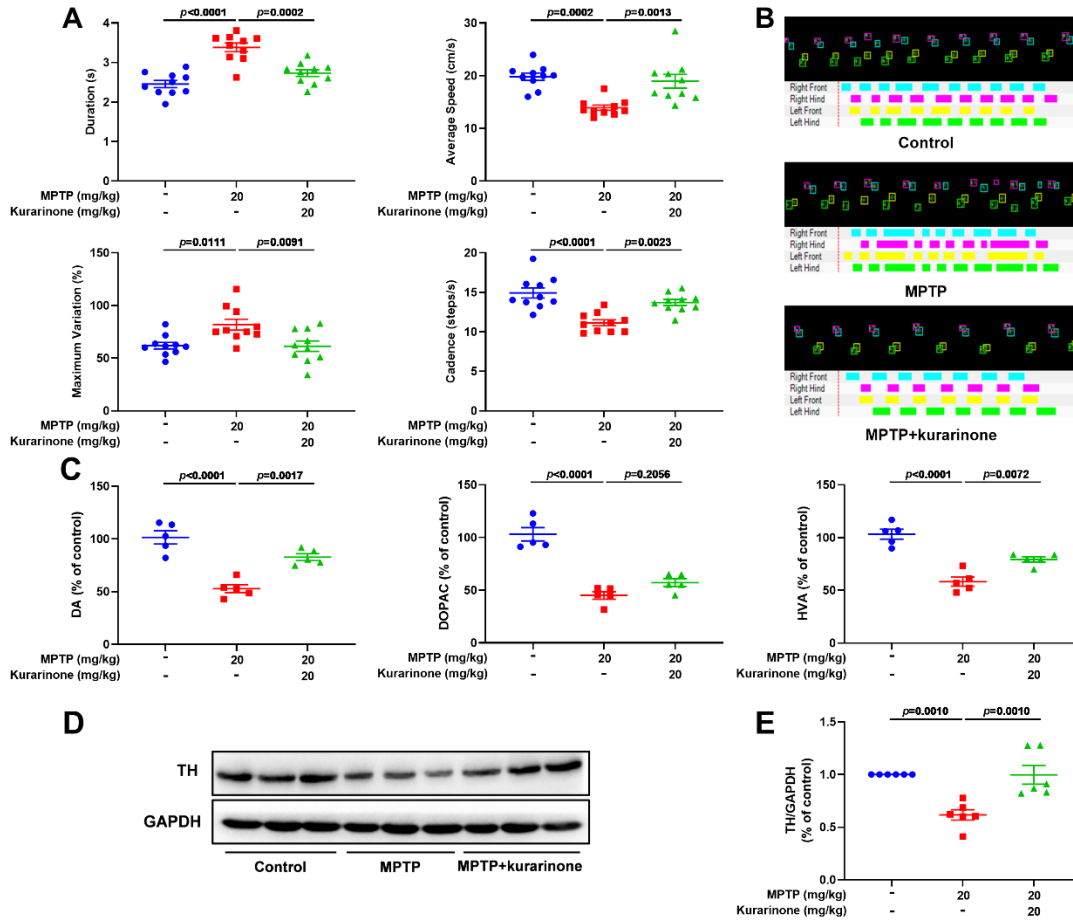


Figure S10 Kurarinone alleviated the behavior of MPTP-induced PD mice after the beginning of MPTP treatment. (A) The behavioristics parameters. Data represent mean \pm SEM, $n = 10$. The significant difference was determined by one-way ANOVA followed by Tukey's test. (B) The representative footprints. The significant difference was determined by one-way ANOVA followed by Tukey's test. (C) Effects of kurarinone on neurotransmitters DA, DOPAC, and HVA after the beginning of MPTP treatment. Data represent mean \pm SEM, $n = 5$. The significance of difference was determined by one-way ANOVA followed by Tukey's test. (D) Effect of kurarinone on TH expression level in SN after the beginning of MPTP treatment. (E) Quantitative data of TH. Data represent mean \pm SEM, $n = 6$. The significance of difference was determined by one-way ANOVA followed by Tukey's test.

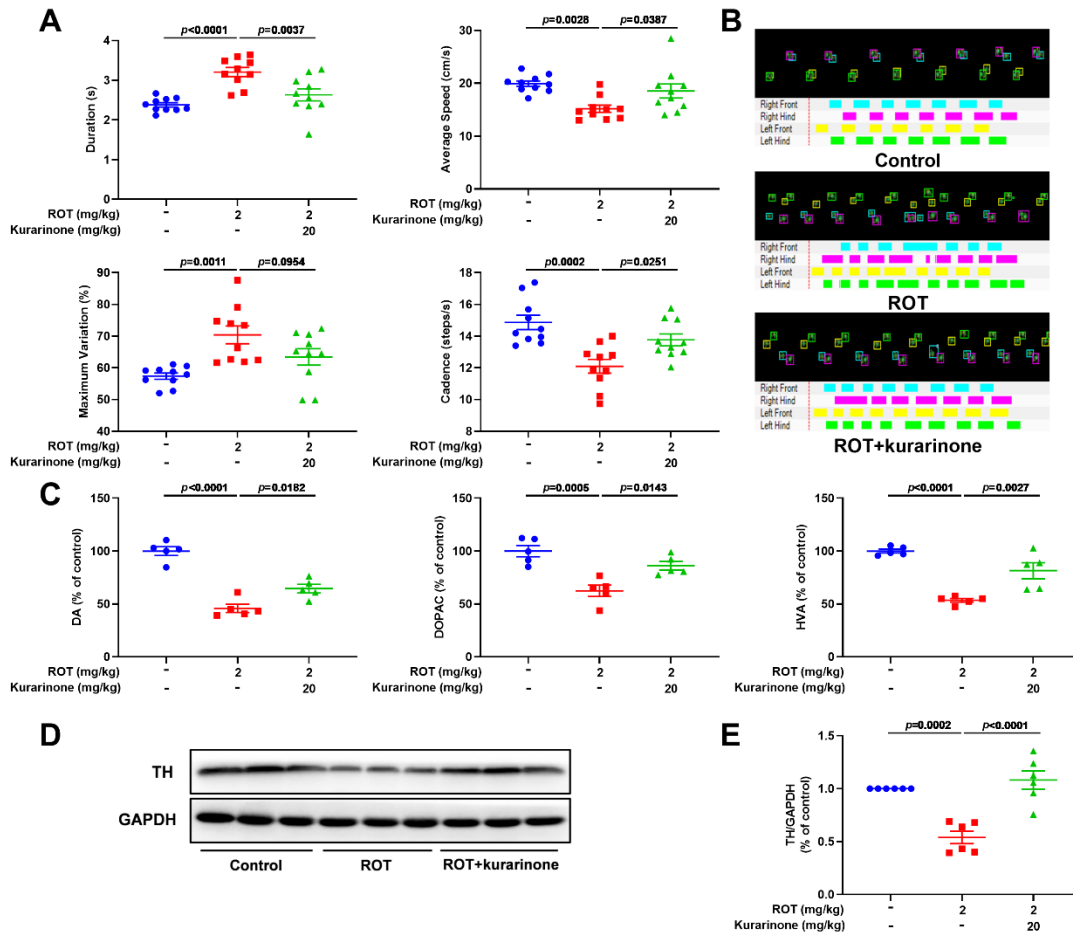
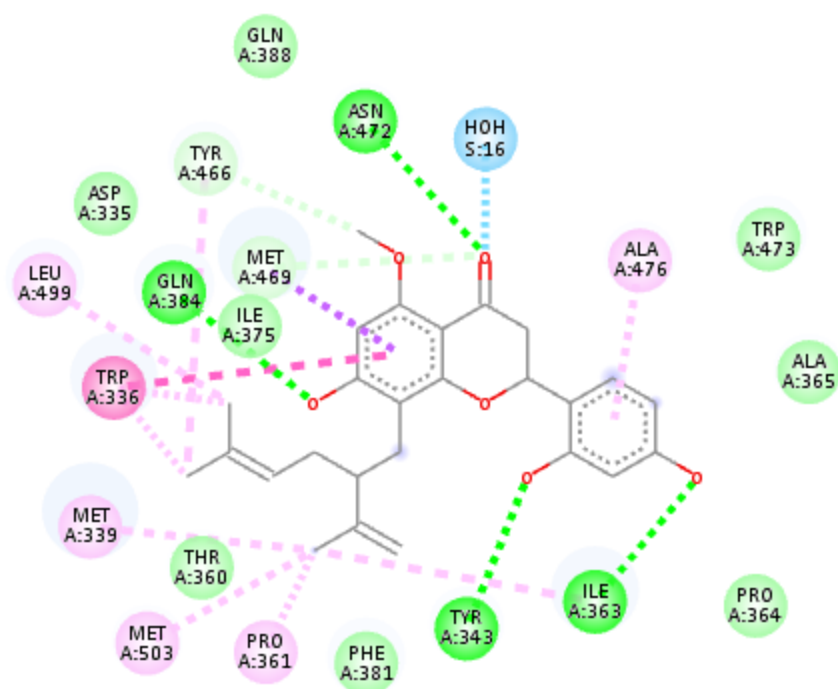


Figure S11 Kurarinone alleviated the behavior of ROT-induced PD mice after the beginning of ROT treatment. (A) The behavioristics parameters. Data represent mean \pm SEM, $n = 10$. The significant difference was determined by one-way ANOVA followed by Tukey's test. (B) The representative footprints. The significant difference was determined by one-way ANOVA followed by Tukey's test. (C) Effects of kurarinone on neurotransmitters DA, DOPAC, and HVA after the beginning of ROT treatment. Data represent mean \pm SEM, $n = 5$. The significance of difference was determined by one-way ANOVA followed by Tukey's test. (D) Effect of kurarinone on TH expression level in SN after the beginning of ROT treatment. (E) Quantitative data of TH. Data represent mean \pm SEM, $n = 6$. The significance of difference was determined by one-way ANOVA followed by Tukey's test.



Interactions

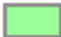





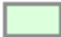

	van der Waals		Pi-Sigma
	Water Hydrogen Bond		Pi-Pi T-shaped
	Conventional Hydrogen Bond		Alkyl
	Carbon Hydrogen Bond		Pi-Alkyl

Figure S12 The interaction of kurarinone with sEH in the 2D plot.

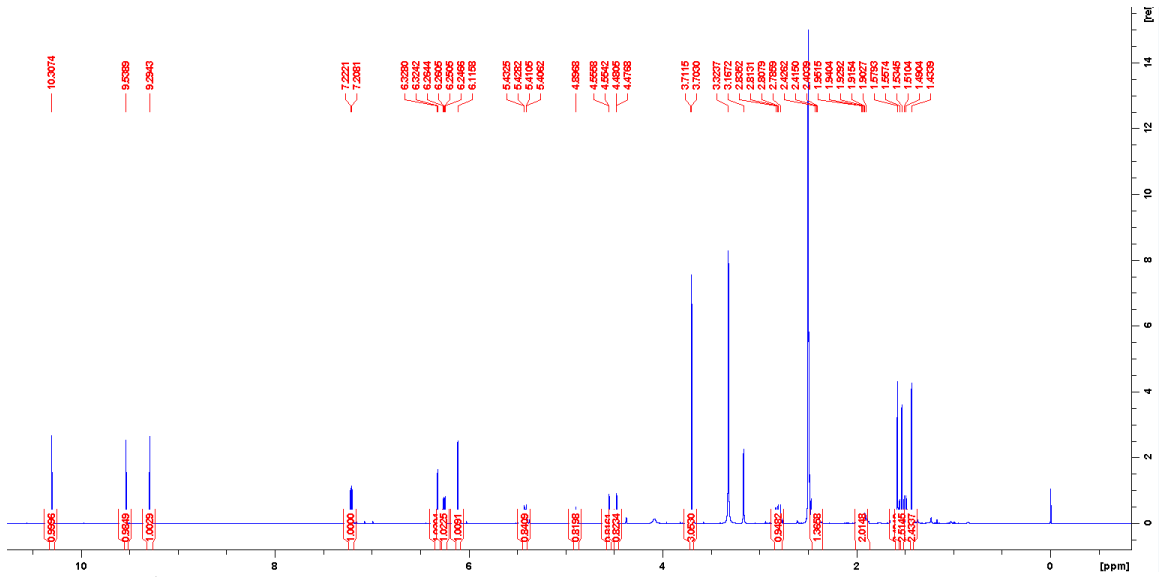


Figure S13 ¹H (600 MHz, DMSO-*d*₆) NMR spectrum of kurarinone

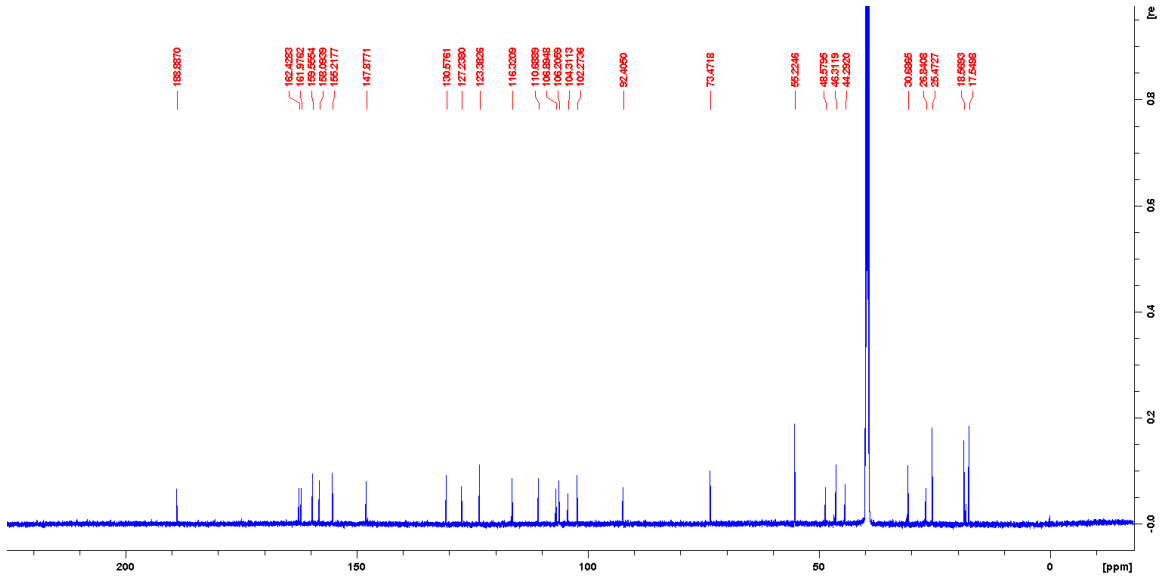


Figure S14 ¹³C (150 MHz, DMSO-*d*₆) NMR spectrum of kurarinone

Table S1. Functional annotation of differential proteins.

ID	Gene Name	GOTERM_BP_DIRECT
Hirip3	HIRA interacting protein 3	
Adgrb1	adhesion G protein-coupled receptor B1	cell surface receptor signaling pathway, G-protein coupled receptor signaling pathway, negative regulation of angiogenesis, positive regulation of synapse assembly
Chd2	chromodomain helicase DNA binding protein 2	transcription, DNA-templated, regulation of transcription, DNA-templated, cellular response to DNA damage stimulus, muscle organ development, covalent chromatin modification, hematopoietic stem cell differentiation
Ccdc9	coiled-coil domain containing 9	
Dsp	desmoplakin	desmosome organization, ventricular compact myocardium morphogenesis, single organismal cell-cell adhesion, peptide cross-linking, keratinocyte differentiation, adherens junction organization, wound healing, skin development, intermediate filament cytoskeleton organization, intermediate filament organization, protein localization to adherens junction, bundle of His cell-Purkinje myocyte adhesion involved in cell communication, regulation of heart rate by cardiac conduction, regulation of ventricular cardiac muscle cell action potential
Ephx2	soluble epoxide hydrolase	prostaglandin production involved in inflammatory response, lipid metabolic process, inflammatory response , metabolic process, response to toxic substance, positive regulation of gene expression, dephosphorylation, sensory perception of pain, aromatic compound catabolic process, cholesterol homeostasis, linoleic acid metabolic process, positive regulation of blood pressure, stilbene catabolic process, phospholipid dephosphorylation, regulation of cholesterol metabolic process
Eif4ebp2	eukaryotic translation initiation factor 4E binding protein 2	regulation of translation, regulation of translational initiation, memory, insulin receptor signaling pathway, negative regulation of translation, cAMP-mediated signaling, TOR signaling, social behavior, negative regulation of translational initiation, regulation of synaptic plasticity, modulation of synaptic transmission
Krt17	keratin 17	morphogenesis of an epithelium, signal transduction, positive regulation of cell growth, hair follicle morphogenesis, keratinization, intermediate filament organization, positive regulation of translation, positive regulation of hair follicle development
Krt6a	keratin 6A	morphogenesis of an epithelium, Wnt signaling pathway, keratinization, wound healing, intermediate filament organization,

Krt79	keratin 79	
Nccrp1	non-specific cytotoxic cell receptor protein 1 homolog (zebrafish)(Nccrp1)	positive regulation of cell proliferation,
Slc18a2	solute carrier family 18 (vesicular monoamine), member 2 (Slc18a2)	response to amphetamine, transport, neurotransmitter transport, chemical synaptic transmission, aging, locomotory behavior, response to toxic substance, post-embryonic development, aminergic neurotransmitter loading into synaptic vesicle, monoamine transport, drug transport, insulin secretion, cellular response to drug, glucose homeostasis, negative regulation of neurotransmitter transport, transmembrane transport,
Smndc1	survival motor neuron domain containing 1	mRNA processing, apoptotic process, RNA splicing,
Tdrp	testis development related protein	spermatogenesis,

Table S2. Inhibition of mouse sEH activity by kurarinone using MNPC as substrate.

Kurarinone		TPPU	
Concentration (μM)	Inhibition ratio (%)	Concentration (μM)	Inhibition ratio (%)
5.0	91.05	5.0	93.43
2.5	86.68	2.5	94.39
1.25	75.08	1.25	91.77
0.625	60.74	0.625	81.41
0.3125	41.69	0.3125	69.25
0.1563	27.72	0.1563	56.68
0.0781	17.02	0.0781	41.58
0.0391	5.68	0.0391	19.98
IC_{50} (nM)	415.2		1.26

Table S3. Inhibition of human sEH activity by kurarinone with t-DPPO a radioactive substrate

[S] = 50 μM		[S] = 5.3 μM	
Kurarinone μM	% Inhibition	Kurarinone μM	% Inhibition
0.25	26.8	0.5	19.1
0.5	39.8	1.0	4.1
1.0	37.8	2.5	3.0
2.5	40.5	5.0	23.2
5.0	73.5	10.0	53.7
IC_{50} (μM)	3.0	IC_{50} (μM)	9.7

Table S4. Inhibition of kurarinone towards human sEH activity with MNPC as a fluorescent substrate

Kurarinone		TPPU	
Concentration (μM)	Inhibition ratio (%)	Concentration (μM)	Inhibition ratio (%)
50	98.1	0.05	96.9
25	98.1	0.025	98.4
12.5	99.7	0.0125	96.0
6.25	94.2	0.00625	91.3
3.125	84.9	0.003125	84.6
1.5625	72.1	0.001563	74.1
0.78125	58.6	0.000781	62.1
0.390625	44.5	0.000391	43.3
IC_{50} (nM)	509.9		0.49

Table S5. Data collection and refinement statistics.

Wavelength	0.979
Space group	P41 (number 76)
a,b,c (Å)	56.7900 56.7900 112.5200
α,β,γ (°)	90.0000 90.0000 90.0000
Resolution (Å)	2.10
No. of observations	129054
No. of unique reflections	18344
Completeness (%)	99.8 (99.8)
$\langle I \rangle / \sigma(I)$	8.7 (2.2)
Redundancy	7.0 (7.2)
R_{merge}	0.214 (1.130)
$R_{\text{p.i.m}}$	0.132 (0.681)
$R_{\text{work}} / R_{\text{free}}$	0.173 / 0.214
No. atoms	2626
Protein	2391
Ligand/ion	3
Water	232
B-factors	
Protein	26.105
Ligand/ion	46.880
Water	33.093
Ramachandran	
Favored (%)	97.69
Allowed (%)	2.31
Outlier (%)	0
R.m.s. deviations	
Bond lengths (Å)	0.0152
Bond angles (°)	1.6447

Table S6. The ^1H (600 MHz, $\text{DMSO-}d_6$) and ^{13}C (150 MHz, $\text{DMSO-}d_6$) NMR data of kurarinone

Position	δ_c	δ_H (J, in Hz)	Position	δ_c	δ_H (J, in Hz)
2	73.5	5.42, dd (13.2, 2.5)	5	106.2	6.25, dd (8.3, 2.2)
3	44.3	2.81, dd (16.1, 13.2) 2.44, dd (16.1, 2.5)	6	127.2	7.21, d (8.3)
4	188.9		1	26.8	2.49, m
4a	159.6		2	46.3	2.48, m
5	162.4		3	30.9	1.93, m
6	92.4	6.12, s	4	123.4	4.90, m
7	162.0		5	130.6	
8	106.9		6	25.5	1.44, s
8a	104.3		7	17.5	1.53, s
1	116.3		8	147.9	
2	155.2		9	110.7	4.56, m
3	102.3	6.33, d (2.2)			4.48, d (2.2)
4	158.1		10	18.6	1.58, s
			5-OCH ₃	55.2	3.70, s

SI References

- [1] Y. Liu, Z. Liu, M. Wei, M. Hu, K. Yue, R. Bi, S. Zhai, Z. Pi, F. Song, Z. Liu, Pharmacodynamic and urinary metabolomics studies on the mechanism of Schisandra polysaccharide in the treatment of Alzheimer's disease, *Food Funct* 10(1), 432-447 (2019).
- [2] W.Y. Zhao, Z.L. Luan, T.T. Liu, W.H. Ming, X.K. Huo, H.L. Huang, C.P. Sun, B.J. Zhang, X.C. Ma, Inula japonica ameliorated bleomycin-induced pulmonary fibrosis via inhibiting soluble epoxide hydrolase, *Bioorg Chem* 102, 104065 (2020).
- [3] C. Morisseau, B.D. Hammock, Measurements of soluble epoxide hydrolase (sEH) activity, *Curr. Protoc. Toxicol.* 33, 4.23.1-4.23.18 (2007).
- [4] Z. Otwinowski, W. Minor, Processing of X-ray diffraction data collected in oscillation mode, *Methods Enzymol* 276, 307-26 (1997).
- [5] A. Kramer, T. Wagner, O. Yildiz, F.J. Meyer-Almes, Crystal Structure of a Histone Deacetylase Homologue from *Pseudomonas aeruginosa*, *Biochemistry* 55(49), 6858-6868 (2016).
- [6] P.D. Adams, R.W. Grosse-Kunstleve, L.W. Hung, T.R. Ioerger, A.J. McCoy, N.W. Moriarty, R.J. Read, J.C. Sacchettini, N.K. Sauter, T.C. Terwilliger, PHENIX: building new software for automated crystallographic structure determination, *Acta Crystallogr D Biol Crystallogr* 58(Pt 11), 1948-54 (2002).
- [7] P. Emsley, K. Cowtan, Coot: model-building tools for molecular graphics, *Acta Crystallogr D Biol Crystallogr* 60(Pt 12 Pt 1), 2126-32 (2004).
- [8] G.N. Murshudov, A.A. Vagin, E.J. Dodson, Refinement of macromolecular structures by the maximum-likelihood method, *Acta Crystallogr D Biol Crystallogr* 53(Pt 3), 240-55 (1997).
- [9] R.A. Laskowski, M.W. MacArthur, D.S. Moss, J.M. Thornton, PROCHECK: A program to check the stereochemical quality of protein structures, *Rev Chim-Bucharest* 26, 283-291 (1993).
- [10] S.Y. Ryu, H.S. Lee, Y.K. Kim, S.H. Kim, Determination of isoprenyl and lavandulyl positions of flavonoids from *Sophora flavescens* by NMR experiment, *Arch Pharm Res* 20(5), 491-5 (1997).